ADVANCED FUNCTIONAL MATERIALS
www.afm-journal.de

Nanoporous Hydrogen Bonded Polymeric Microparticles: Facile and Economic Production of Cross Presentation Promoting Vaccine Carriers

*Marijke Dierendonck, Kaat Fierens, Riet De Rycke, Lien Lybaert, Samarendra Maji, Zhiyue Zhang, Qilu Zhang, Richard Hoogenboom, Bart N. Lambrecht, Johan Grooten, Jean Paul Remon, Stefaan De Koker, and Bruno G. De Geest**

Nanoporous microparticles are produced in a single step based on hydrogen bonding between a neutral polymer and tannic acid. These particles are stable in physiological medium, are non-toxic to in vitro cultured cells, and can efficiently encapsulate proteins. In vitro and in vivo experiments show that these porous hydrogen bonded microparticles are able to induce antigen-specific cellular and humoral immune responses against encapsulated vaccine antigens. Considering the easy and low cost manufacturing of this dry powder formulation from approved readily available components, it is anticipated that this technology holds great promise for the formulation of vaccines for developing countries or for pandemic vaccines where long term storage under refrigerated conditions is a major issue. Additionally, due to the versatility of the approach facilitates straightforward co-encapsulation of a wide variety of additional components to further modulate the immune response.

1. Introduction

Strategies that allow fast and efficient encapsulation of proteins into hydrophilic and fully hydrated microparticles are of great interest for a number of applications in biotechnology, diagnostics, and biomedicine.[1–3] When envisioning intracellular delivery of vaccine antigens, such particles are particularly advantageous. Particles in the 0.1–10 μm size range mimic the dimensions of micro-organisms and are consequently readily recognized and internalized by dendritic cells, the main antigen presenting cells and inducers of adaptive immunity.[4–6] Once internalized, particulate antigens will be processed in the phagosomes and presented as MHC-peptide complexes to T cells. Particulate antigens are generally presented via MHCI and MHCII, enabling thereby the simultaneous induction of CD8 and CD4 T cell responses. In the appropriate inflammatory context, MHCI-peptide stimulated CD8 T cells will differentiate into cytotoxic T cells possessing the unique capacity to recognize and kill infected or transformed cells. This path of the immune response is termed cellular immunity and is tought to be crucial for effective vaccination against intracellular pathogens such as HIV, malaria, tuberculosis, and so forth, and for anticancer immune therapy.[7] CD4 T cells stimulated by MHCII-peptide complexes can differentiate into distinct T helper subsets, which support B cells to produce antibodies that mobilize innate immune cells to combat pathogens. In contrast to particulate antigens, presentation of soluble antigens is almost entirely restricted to the MHCII pathway. As a consequence, soluble antigens will largely fail to evoke CD8 T cell responses.

Thus currently, there is major interest in the development of adjuvant systems that stimulate cellular immune responses via formulation in nano- and microparticles.[8–15] In this regard it is crucial to use materials and procedures that are biologically friendly and scalable from the laboratory to industry. Here we present an all aqueous one-step method to produce antigen loaded microparticles using hydrogen bonding as driving force for particle assembly. Based on our previous work[16–18] using oppositely charged polyelectrolytes that assembly via electrostatic interaction,[19–21] we apply atomization into air of diluted aqueous liquid containing antigen, H-bonding matrix-forming components, and mannitol as pore-forming component. This spray drying process yields solid microparticles with sub 10 μm

M. Dierendonck, L. Lybaert, Z. Zhang, Prof. J. P. Remon, Prof. B. G. De Geest
Department of Pharmaceutics
Ghent University
9000, Ghent, Belgium
E-mail: br.degeest@ugent.be
K. Fierens, R. De Rycke, Prof. B. N. Lambrecht
VIB Inflammation Research Center
9052 Zwijnaarde, Belgium
K. Fierens, Prof. B. N. Lambrecht
Department of Respiratory Medicine
Ghent University
9000 Ghent, Belgium
Dr. S. Maji, Q. Zhang, Prof. R. Hoogenboom
Supramolecular Chemistry Group
Department of Organic Chemistry
Ghent University
9000 Ghent, Belgium
Prof. J. Grooten, Dr. S. De Koker
Department of Biomedical Molecular Biology
Ghent University
9052 Zwijnaarde, Belgium

DOI: 10.1002/adfm.201400763

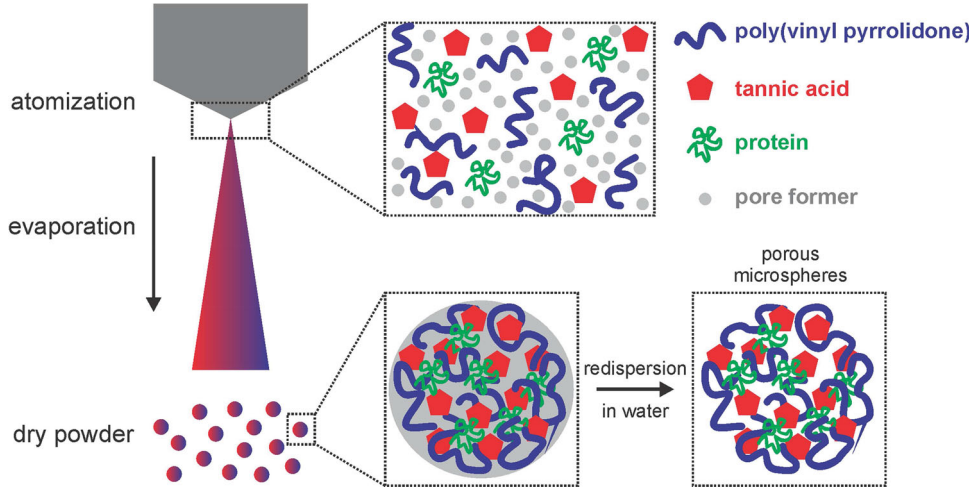

Scheme 1. Schematic representation of the encapsulation of protein antigen in porous microparticles based on H-bonding interacting species. As pore-former mannitol is used which instantaneously dissolves upon redisperion in aqueous medium, thereby creating a highly porous matrix.

dimension, to assure phagocytocis by DCs. Owing to its dry state, this formulation has particularly advantages for long time storage and transportation under non-refrigerated conditions, which is of major importance for pandemic vaccines and vaccines intended for the developing world.[22] The role of the pore-forming component in the formulation, is to create a nanoporous internal network within the microparticles upon redispersion of the particles in aqueous medium. As mannitol is highly water-soluble it will immediately dissolve, that is, leach out of the particles, thereby creating porosity. The process to fabricate such microparticles is schematically depicted in **Scheme 1**. Our hypothesis is that microparticles with a nanoporous interior, unlike monolithic particles, allow a more profound diffusion by intracellular proteases upon cellular uptake. This is expected to lead to a faster and more efficient processing and presentation of the full antigen payload.

As complementary H-bonding components we use tannic acid (TA; **Scheme 2**A) as hydrogen bond donor and poly(*N*-vinylpyrrolidone) (PVP; Scheme 2B) as hydrogen bond acceptor.[23] PVP is a neutral polymer that is available as pharma-grade and is allowed by the FDA as excipient for injectables. TA and PVP are known to form strong H-bonded complexes that remain stable over a wide pH range.[24–26] Whereas, TA has been used for self-asembly,[27] including planar multilayer films and capsules via hydrogen bonding[28–31] and coordination complex formation,[32] the fabrication of microparticles by simply spraying species that interact via hydrogen bonding has, to the best of our knowledge, not yet been reported so far. Importantly, as polycations are generally regared as cytotoxic, developing systems that can replace electrostatic interaction by hydrogen bonding are of stong interest for the biomedical field.[33,34]

2. Results and Discussion

2.1. Assembly of Nanoporous Hydrogen Bonded Microparticles

In this study, we used commercially available PVP, branded as Kollidon12, which is available as endotoxin-free grade. As stated by the manufacturer, it has a molecular weight of 2–3 kDa, which was determined in our lab by SEC to be $M_{n,SEC}$ 1.8 kDa ($Đ$ = 1.89), relative to PMMA standards, for that specific lot which was used during the whole study. As the molecular weight of the polymer is considerably lower compared to polymers that are commonly used in multilayer build up (i.e., typically around 50 kDa), we evaluated whether this PVP was capable to form stable assemblies with TA via Quartz Crystal Microbalance (QCM). Therefore, a gold coated quartz chip was pre-conditioned by adsorption of a monolayer of mercaptosuccinnic acid, inducing a negative surface charge, followed by a cationic poly(ethylene imine) (PEI) layer to promote further Layer-by-Layer (LbL) assembly. Subsequently, the multilayer build-up was started by injecting TA into the flow cell, followed by an adsorption time

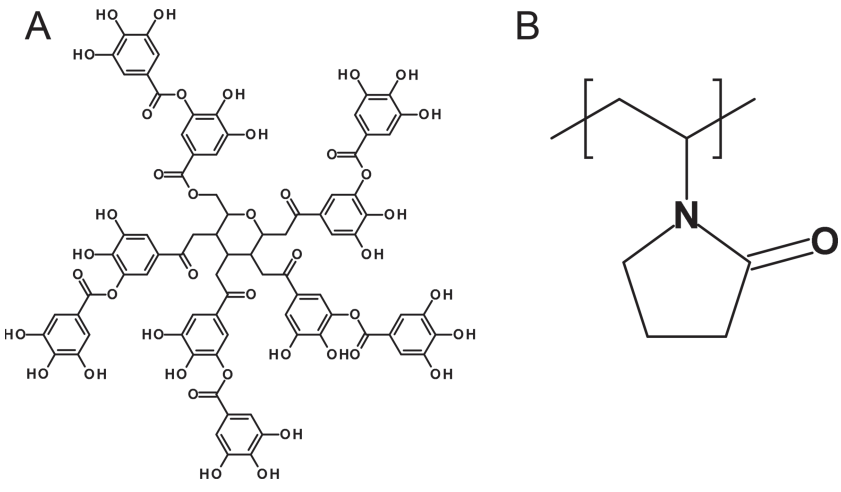

Scheme 2. Molecular structure of A) tannic acid (TA), and B) poly(N-vinylpyrrolidone) (PVP).

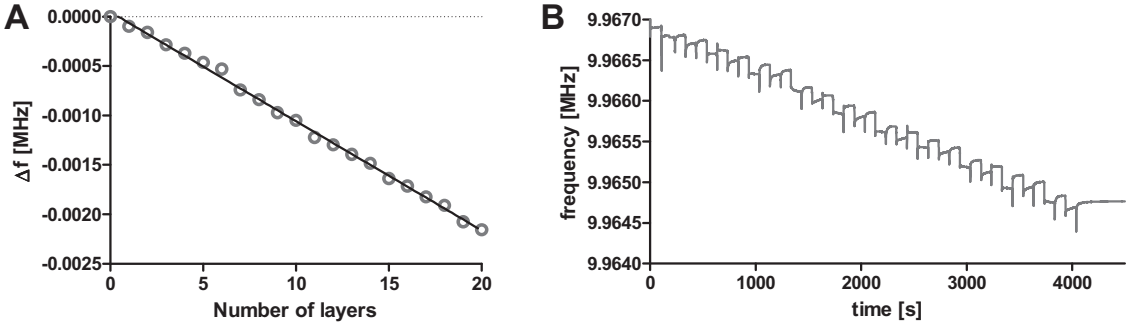

Figure 1. A) QCM trace during assembly of a 10 TA/PVP bilayer film. B) Decrease of the resonance frequency (Δf) as function of the deposition steps.

of 100 s to reach a stable value of the resonance frequency. A rinsing step with demi water was applied to remove non-adsorbed and weakly adsorbed TA from the flow cell and next PVP was injected. Immediately a drop in resonance frequency took place that levelled of within 100 s, then again followed by a washing step with demi water to remove unadsorbed and weakly adsorbed species. This procedure was repeated until a total of 10 TA/PVP bilayers was assembled. The raw data of the QCM signal shown in **Figure 1**A, depicts a steady decrease of the resonance frequency upon every adsorption step, with only a minor increase in resonance frequency upon each rinsing step. When plotting the evolution of resonance frequency as function of the number of deposited layers (Figure 1B), a linear decrease is observed indicating successful consecutive LbL build-up. These findings were confirmed by monitoring multilayer assembly (with intermittent drying) on quartz substrates with UV-VIS spectroscopy (data not shown). More general, this means that PVP with a relatively low molecular weight is able to form stable hydrogen bonded complexes with TA. These data are in accordance to earlier reports, albeit that PVP with a significantly higher molecular weight was used.[24]

Encouraged by these findings, we proceeded with evaluating the formation of TA/PVP microparticles via an atomization-evaporation (i.e., spray drying) set up. Previously we have reported on the formation of porous particles composed of oppositely charged polyelectrolytes that form a stable complex via electrostatic interaction.[16–18] Proteins such as vaccine antigens and enzymes could, very efficiently, be entrapped within this polyelectrolyte network and key in assuring preservation of the biological activity of these proteins was the use of mannitol as pore-forming component mixed with the polyelectrolytes and proteins prior to spray drying.[17] Mannitol is FDA approved and highly water-soluble, thereby immediately dissolving and leaching from the particles upon redispersion in aqueous medium. Additionally, mannitol is often used in the pharmaceutical industry to enhance the overall yield of the spray drying process due to its excellent flow properties.[35] Therefore, in the current study, we prepared a diluted aqueous dispersion of mannitol, PVP and TA under constant stirring to avoid the formation of large precipitates. The ratio's of these components were chosen based on our previous findings for polyelectrolyte based microparticles as listed in **Table 1**.[16,17] The mixture was fed to the nozzle of the spray drier and atomized into a heated air stream. After evaporation of the water, the resulting solid particles were collected via a cyclone and stored for further studies.

Table 1. Composition of the OVA formulations.

Sequence					ratio [wt%]
1	mannitol	OVA	PVP	TA	40/1/10/10
2	mannitol	PVP	TA	OVA	40/10/10/1
3	mannitol	OVA	TA	PVP	40/1/10/10

2.2. Particle Characterization

The obtained microparticles were characterized in the dry state by scanning electron microscopy (SEM) and after rehydration in aqueous medium by laser diffraction and transmission electron microscopy (TEM). The SEM images in **Figure 2**A demonstrate that spherically shaped microparticles, with diameters in the dry state below 10 μm, are obtained via the spray drying process. Optical microscopy (Figure S2, Supporting Information) verifies that the microparticles remain stable upon redispersion in phosphate buffered saline (PBS) without agglomerating or disassembling, indicating that the hydrogen bonds between the TA and PVP are strong enough to form stable particles in water without inter-particle aggregation to occur. This is further confirmed by laser diffraction in wet state, showing a monomodal particle size distribution between 1–10 μm and a volume mean particle diameter of 4.02 ± 0.25 μm (Figure 2B). Analysis of the SEM images by Image J yielded a number mean particle diameter of 1.04 ± 0.65. This is markably lower than the size distribution obtained via laser diffraction. However it is important to consider the fact that laser diffraction was measured on particles in a swollen hydrated state whereas SEM was performed on dry particles. Additionally the volume mean diameter calculated by laser diffraction is strongly affected by larger particles, which thus accounts for the larger mean diameter measured by laser diffraction relative to the number mean diameter measured by SEM. These are important findings in view of applying these particles as intracellular vaccine carriers where particle sizes below 10 μm are required for efficient phagocytosis by antigen presenting cells. To assess the internal structure of the TA/PVP microparticles, they were embedded in an epoxy matrix and cut into ultrathin slices via ultramicrotomy. Subsequent TEM imaging revealed a highly porous internal structure as depicted in Figure 2C. The porosity of the microparticles and the role of mannitol to induce this porosity was further verified by comparing SEM images (Figure S3, Supporting Information) before

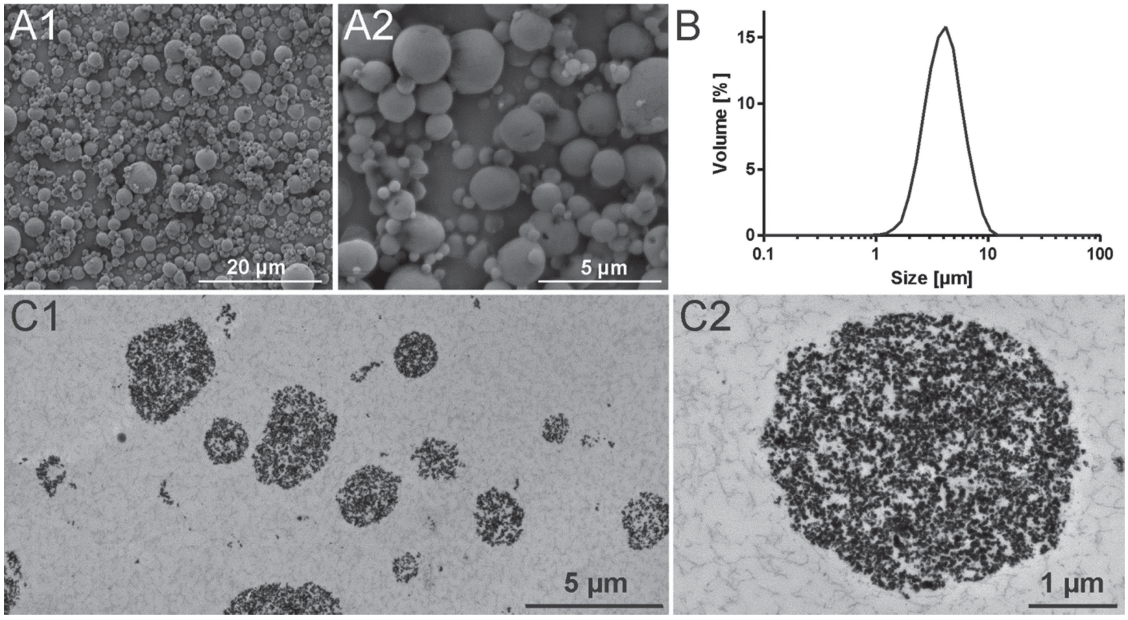

Figure 2. A) Scanning electron microscopy images of the microparticles obtained in dry state after spray-drying. B) Size distribution of the microparticles measured by laser diffraction after redispersion in aqueous medium. C) Transmission electron microscopy images (recorded from microtomed epoxy-embedded microparticles), depicting the high internal porosity of the microparticles after redispersion in water.

and after redispersion in water. These observations unambiguously proves the formation of a highly porous internal network structure within the TA/PVP microparticles after removal of mannitol. Image analysis of the TEM images on 20 individual particles revealed a pore volume of 36 ± 11%.

In a next series of experiments we investigated to which extend such TA/PVP microparticles can encapsulate protein antigens. Therefore, ovalbumin (OVA; chicken egg albumin with a molecular weight of ~43 kDA) was used as model antigen. Ovalbumin is a relatively inert antigen containing both a MHCI and a MHCII peptide epitope recognized in the C57/Bl6 mice strain. In addition, a large set of murine-based immunological tools are available to characterize the performance OVA-based vaccine formulations. OVA was added to the aqueous mixture of TA, PVP and mannitol prior to spray drying. As TA will also partly complex to OVA via a combination of hydrogen bonding and hydrophobic interactions,[36] we analysed whether the sequence of mixing OVA, TA and PV prior to spray drying has an influence on the extent to which OVA will be retained within the microparticles upon redispersion in aqueous medium (i.e., as "encapsulation efficiency").

To measure to which extend OVA remains entrapped within the TA/PVP matrix upon redispersion of the particles in aqueous medium (i.e., phosphate buffered saline (PBS)), we centrifuged the microparticles and determined the OVA concentration in the supernatant. Therefore, we used fluorescently labelled (i.e., AlexaFluor488) OVA as the presence of TA would interfere with every available protein assay. Additionally, to provide full characterization of the particles also the release of TA and PVP in the supernatant was measured. Owing to its multitude of aromatic groups, TA can easily be detected by UV-VIS spectroscopy. Fluorescently labelled PVP was synthesized via MADIX/RAFT polymerization[37] followed by end group modification with fluorescein. As depicted in **Scheme 3**, this labeling was performed by aminolysis of the xanthate group of the PVP, resulting form the chain transfer agent, into a thiol and subsequent Michael addition type thiol-ene conjugation with fluorescein-o-acrylate.[38] To assess whether the fluorescein group

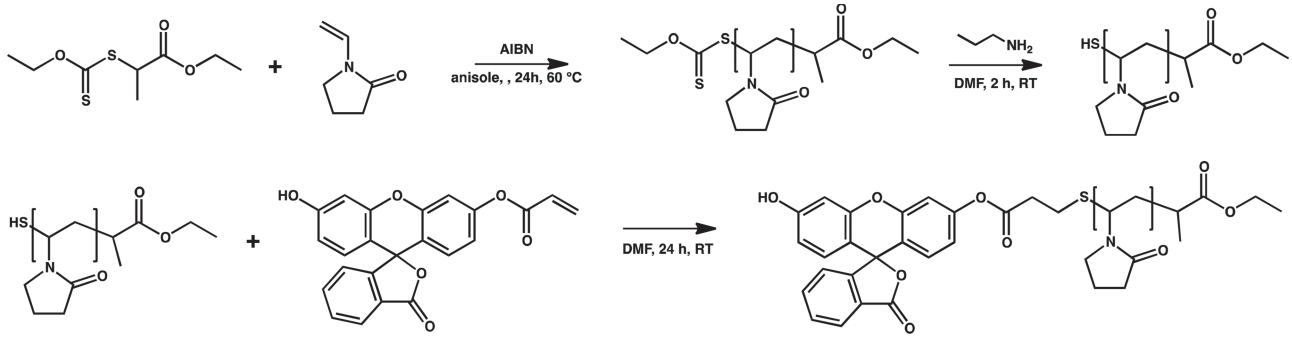

Scheme 3. Reaction scheme of the RAFT/MADIX polymerization of NVP and subsequent fluorescent labeling via thio-ene chemistry of the thiol endgroup to the acrylate group of fluorescein acrylate.

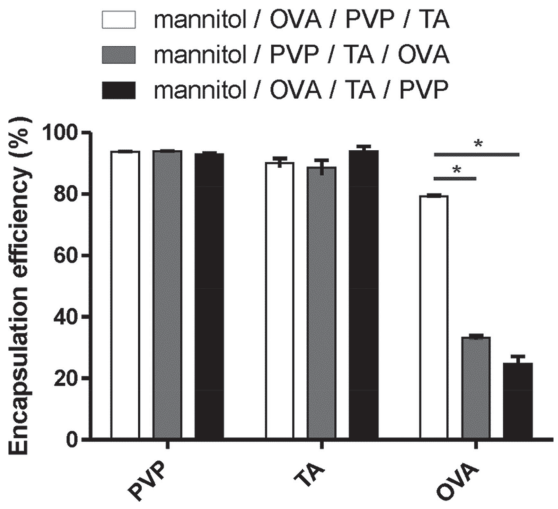

Figure 3. Encapsulation efficiency of PVP, TA, and OVA within the porous microparticles upon redispersion in phosphate buffered saline. Three different mixing sequences of the components were evaluated. (*: $p < 0.05$)

was indeed conjugated to the polymer, size exclusion chromatography (SEC) analysis was performed using a diode array detector (DAD). As shown in Figure S1 (Supporting Information), the UV-VIS absorption spectra recorded at the retention times of PVP clearly reveal the coelution of fluorescein with the PVP proving the covalent linkage. To measure the encapsulation efficiency of respectively the protein, TA and PVP, the microparticles were redispersed in phosphate buffered saline (PBS) followed by vigorous mixing and centrifugation. Next the supernatant was withdrawn and measured to determine the content of the respective components. **Figure 3** summarizes the encapsulation efficiency of the different formulations, expressed as the fraction (in%) of the respective components present in the feed mixture prior to spray drying, that is retained within the microparticles upon redispersion in PBS. These data show that PVP and TA remain largely entrapped within the microparticles upon redispersion in PBS, irrespective of the sequence in which the components are mixed, as in all cases only ≈10% of TA and PVP is released in the medium. However, the encapsulation efficiency of OVA strongly depends on the mixing sequence. On average 80% of the OVA is retained within the microparticles when TA is added last. In the other two cases, a significantly lower amount of OVA (i.e., 20 – 30%) remains entrapped within the microparticles upon redispersion in PBS. When TA is added last, the TA will complex simultaneously with OVA and PVP, allowing a better interaction of the OVA with TA compared to the situation where PVP and TA are mixed prior to addition of OVA. In this case, the strong interaction of PVP with TA likely hampers further complexation of TA with OVA. Why mixing TA with OVA prior to addition of PVP results in a low encapsulation efficiency is less clear. Possibly, TA-bound OVA becomes displaced when a large excess of a PVP is added, forming predominantly TA-PVP complexes (as all three routes yield similar values for the entrapment of TA and PVP) and prevents stable entrapment of OVA into the microparticles upon spray-drying. We also found that the microparticles remain relatively stable during prolongued incubation at physiological conditions (i.e., PBS buffer (pH 7.4 and 0.15 M NaCl), 37 °C), with only a minor fraction of OVA and TA beign released from the microparticles (Figure S4, Supporting Information).

2.3. In Vitro Evaluation

2.3.1. Cellular Uptake

Subsequently, TA/PVP(OVA) microparticles were evaluated in a series of in vitro assays. First, we assessed whether these particles can be internalized by dendritic cells (DCs). Therefore DC2.4 cells were incubated with microparticles containing green fluorescently labelled OVA-AF488 (AF: AlexaFluor). Confocal microscopy was used to visualize particle uptake. To unambiguously discriminate between internalized particles and particles sticking to the cell wall we counterstained cell nuclei with Hoechst and the cell membrane with AF646 conjugated cholera toxin subunit B. By focussing the confocal plane on both the cell nuclei and cell membrane it is straightforward to consider particles as being internalized when they fall between the enclosure of the cell membrane. As shown in **Figure 4**A via flow cytometry and in Figure 4B via confocal microscopy, the microparticles are massively internalized by DCs.

2.3.2. Cytotoxicity

Next, we assessed whether these particles and their components exhibit any cytotoxic effect (**Figure 5**). For this purpose, DC2.4 dendritic cells were incubated with different concentrations of microparticles and their respective individual constituents. Culture medium and DMSO were used as respectively negative and positive controls. Mannitol, OVA and PVP induced no cytotoxicity even at elevated concentrations as high as 1 mg/mL. TA does show cytotoxicity at 1 mg/mL and 0.1 mg/mL, but not at 0.01 mg/mL. The microparticles on their turn only showed toxicity at 1 mg/mL concentrations. However, it has to be noted that at these elevated concentrations, the cells in the 96 well plate are fully covered with particles, thereby limiting diffusion of nutrients and mechanically damaging the cells. Obviously, the in vivo situation will be different, not involving the above mentioned constraints and thereby likely to be tolerant to relatively high particle concentrations.

2.3.3. Cross-Presentation of Encapsulated Antigen

To assess whether encapsulation of OVA in TA/PVP microparticles via spray drying still allows OVA to be processed upon cellular uptake and, particularly, whether cross-presentation to CD8 T cells is promoted, we performed an in vitro CD8 T cell presentation assay. For this purpose, mouse bone marrow derived DCs were pulsed with different concentrations of either soluble or encapsulated OVA and subsequently co-cultured with OT-I cells. OT-I cells are CD8 T cells isolated from transgenic mice having a single T-cell receptor recognizing the MHCI epitope of OVA(SIINFEKL). Prior to culturing them with DCs, OT-I cells are fluorescently labelled with CFSE, which is

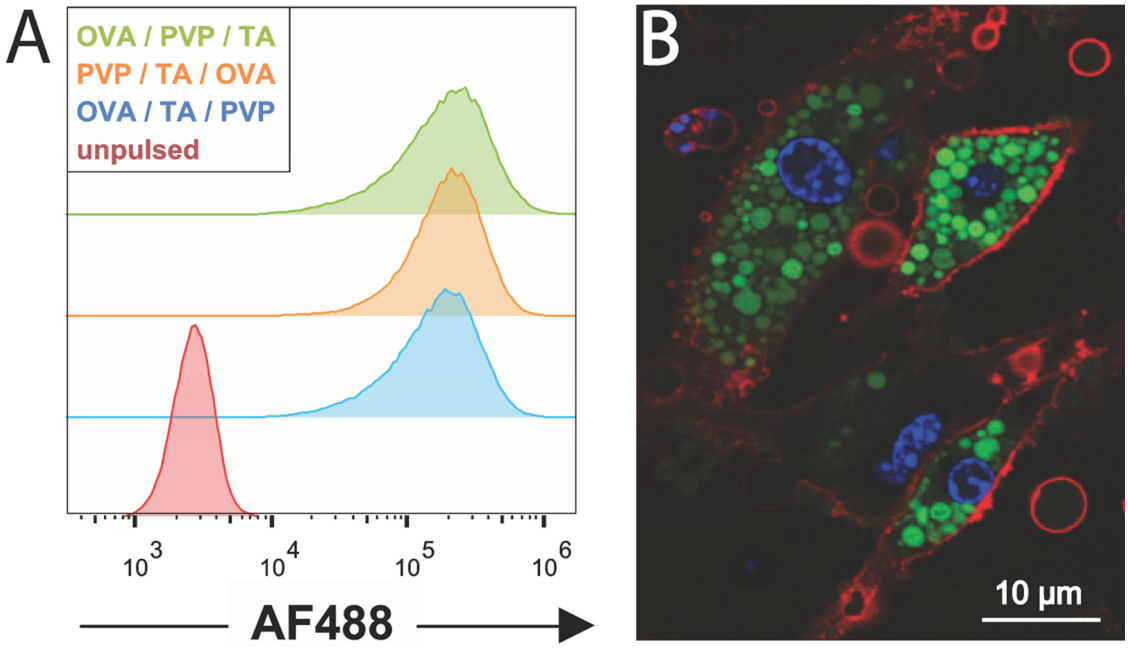

Figure 4. A) Flow cytometry histograms of DC2.4 cells pulsed in vitro with microparticles (containing AF488-conjugated OVA). B) Confocal microscopy image of DC2.4 cells pulsed with OVA/PVP/TA microparticles. Note that the other particles yielded similar images. Cell nuclei were stained blue with Hoechst, the cell membrane with AF647-conjugated cholera toxin subunit B and microparticles containing AF488-conjugated OVA (green fluorescence).

a membrane permeable dye that becomes metabolized into a non-membrane permeable variant by cytoplasmic enzymes. If OVA is presented by DCs via MHCI, CFSE labelled OT-I cells will start to divide. Monitoring the decrease of the fluorescence from mother to daughter OT-I cells by flow cytometry offers a means to measure the quality of antigen cross presentation.

Figure 6A depicts the gating strategy applied to assess transgenic CD8 T cell proliferation. Cells were first gated on living cells, then on T cells and subsequently on CD8 T cells. The flow cytometry histograms in Figure 6B correspond to a DC to T cell ratio of 1:20, and clearly indicates that soluble OVA fails to induce OT-I proliferation at any of the tested OVA concentrations. The graph in Figure 6C shows that at all DC:T cell ratios addressed, no significant response to soluble OVA was detectable. Additionally, we verified that empty (i.e., non-OVA containing) microparticles did not induce T cell proliferation by themselves (Figure S5, Supporting Information). Contrary, encapsulated OVA strongly induced T cell proliferation with a clear dose-dependent trend being observed on the flow cytometry histograms for both antigen concentration and DC to T cell ratio. Indeed, OVA concentrations as low as 0.2 µg/mL induced T cell division only to a slight extend. Higher OVA concentrations such as 2 µg/mL induced strong T cell division for DC to T cell ratios of 1/20 and less. The quantification of T cell proliferation (i.e., percentage of divided OT-I cells) shown by the graphs in Figure 6C for different OVA concentrations and different DC:T cell ratios confirms the trends observed in the flow cytometry histograms, showing a dramatic increase in T cell proliferation when DCs were pulsed with encapsulated versus soluble OVA. Subtle differences are visible between the different types of microparticles with PVP/OVA/TA particles eliciting superior T cell proliferation at the 2 µg/mL dosis. As discussed earlier, these particles retain the highest amount of encapsulated OVA following redispersion in PBS, which probably underlies their superior capacity to stimulate T cell division. This again attributes to the importance of engineering soluble antigens into a particulate form to enhance the cross-presentation efficiency of exogenous antigen to CD8 T cells.

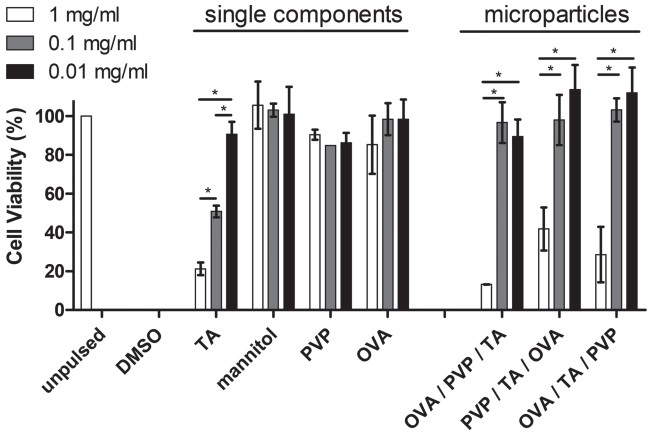

Figure 5. Cell viability measured by MTT assay performed on DC2.4 cells of the microparticles and their respective components. Pure cell culture medium and DMSO were used as negative and positive control, respectively. ($n = 6$; *: $p < 0.05$)

2.4. In Vivo Evaluation

Once confirmed in vitro that encapsulation of antigen in TA/PVP particles still allows antigen to be processed and presented by DCs to T cells, we aimed to assess the capability of our vaccine formulation strategy to enhance the antigen-specific cellular

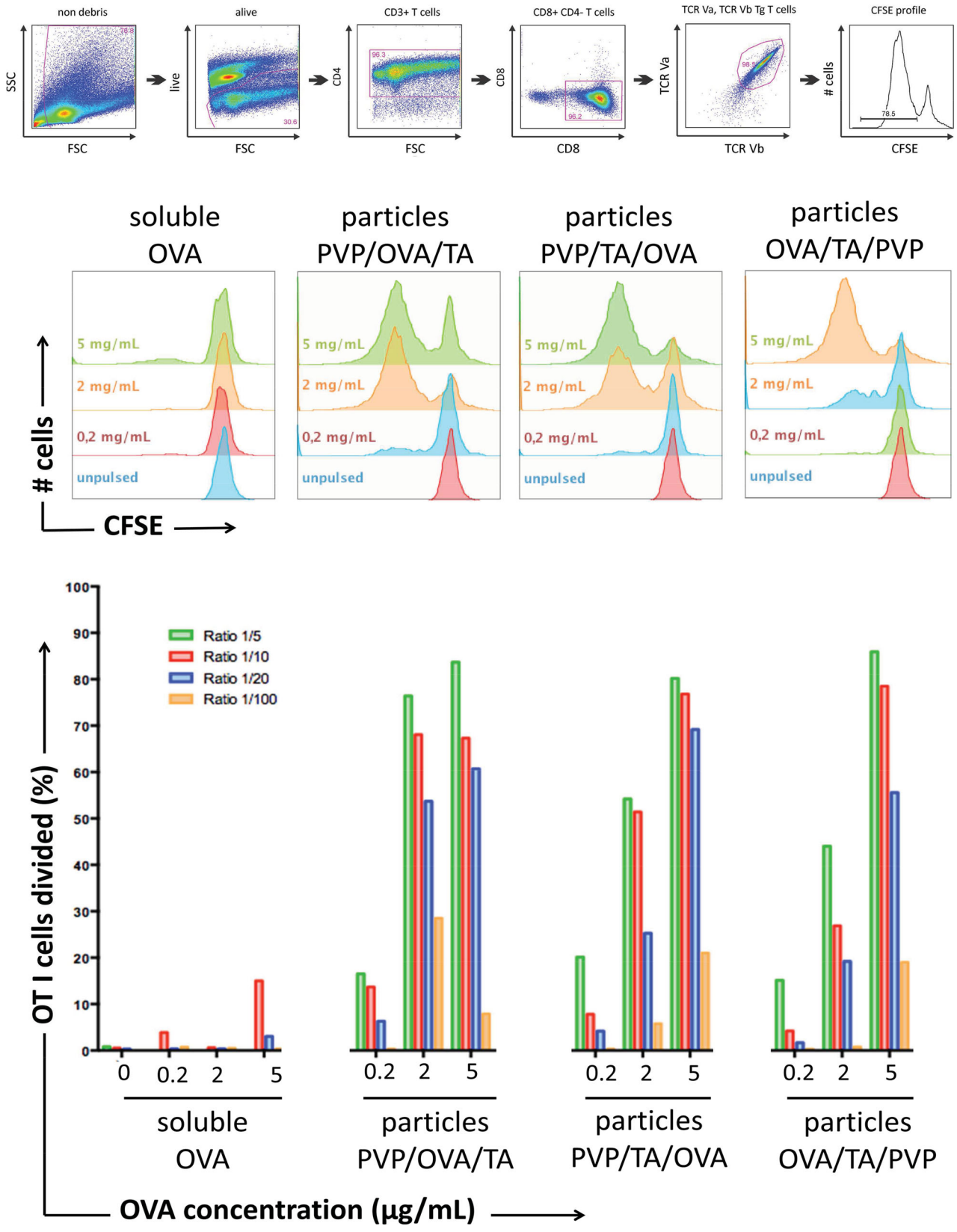

Figure 6. A) Flow cytometry gating strategy to assess OT-I cell proliferation. B) Flow cytometry histograms of OT-I proliferation in response to co-culturing with DCs pulsed with soluble OVA or encapsulated OVA at different OVA concentration. The OT-I cell to DC ratio 1:20. C) Quantitative representation of OT-I cells division as shown in the gating strategy in panel (A).

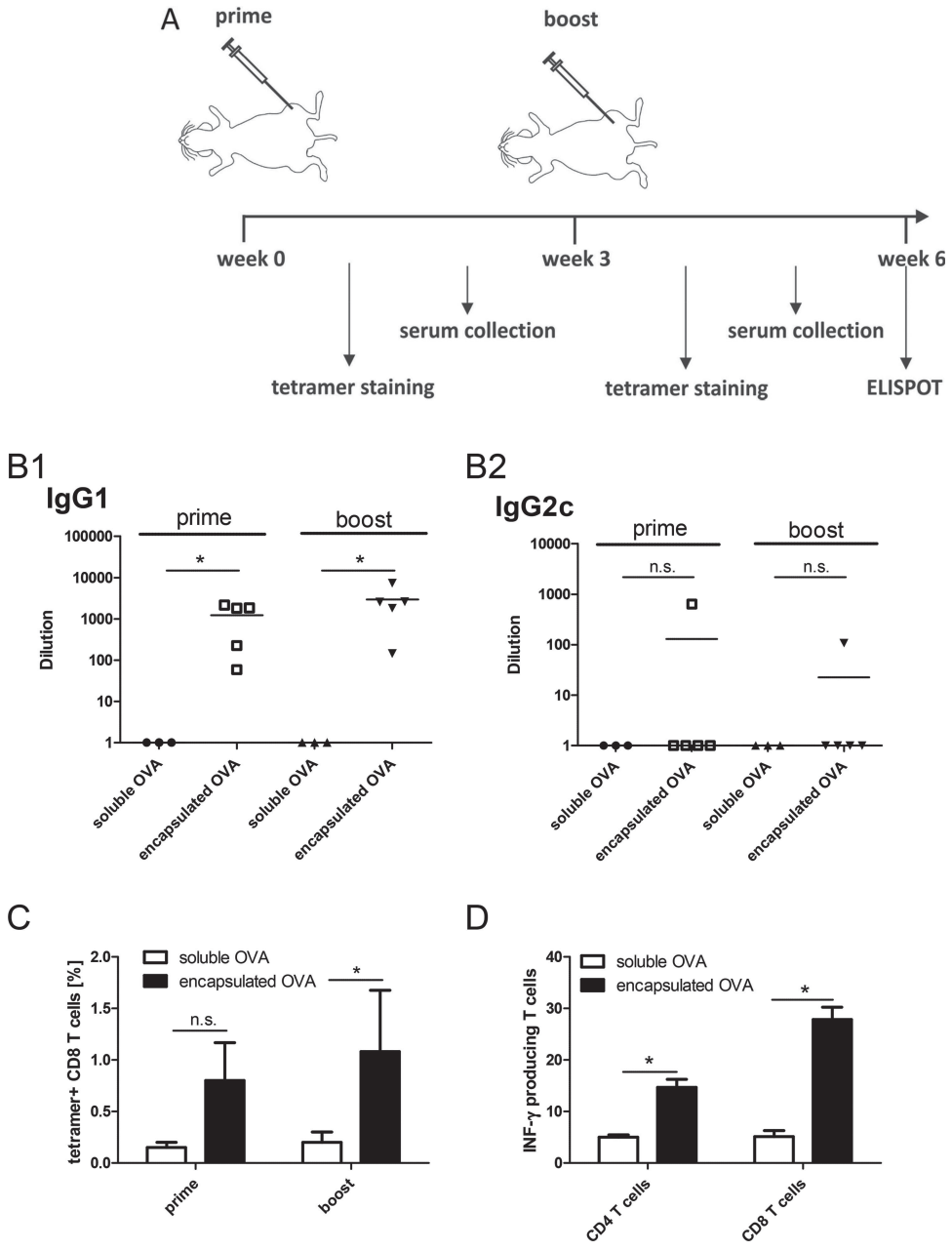

Figure 7. A) Schematic representation of the experimental set-up of the immunization protocol and read out of the humoral and cellular immune response. B) Antibody titers in serum. C) Tetramer positive CD8 T cells in blood. D) INF-γ secreting CD4 and CD8 T cells in the spleen. (n = 5; *: $p < 0.05$))

and humoral immune responses in vivo. As the PVP/OVA/TA particles exhibited the highest OVA encapsulation efficiency (thus providing a more defined system), and were most potent in stimulating CD8 T cell proliferation in vitro, we restricted the experimental set-up for the in vivo experiments to only one microparticle formulation, thereby also reducing the turnover of laboratory animals. Mice (in cohorts of 5) were immunized with either soluble OVA or encapsulated OVA following a prime-boost scheme with a 3 week time interval. Subsequently, the humoral immune response was quantified by measuring anti-OVA antibody titers in serum via enzyme-linked immunosorbent assay (ELISA), while the cellular immune response was quantified by measuring OVA-specific CD8 T cells in blood samples and the induction of INF-γ secreting CD4 and CD8 T cells in the spleen. **Figure 7**A summarizes the experimental set-up. As shown in Figure 7B, relative to soluble antigen, a more than 1000 fold increase in IgG1 was observed for the microparticulate formulation while IgG2c titers were not significantly enhanced. The same trend was observed after the prime and the booster immunization. Tetramer staining on blood samples (Figure 7C) showed an increase in CTLs in the bloodstream. ELISPOT (Figure 7D) analysis of the spleens

showed that also the numbers of both INF-γ secreting CD4 and CD8 T cells were significantly increased when mice were vaccinated with encapsulated rather than soluble antigen, with primarily the CD8 T cell arm of the immune response being enhanced.

3. Conclusion

In conclusion we have shown in this paper that spray drying of TA and PVP with mannitol is a facile, efficient and cheap method to encapsulate co-spray dried vaccine protein antigens. Due to the strong hydrogen bond interaction between TA and PVP the particles retain their spherical morphology upon redispersion in aqueous medium, and stably entrap their payload. Importantly, mannitol acts as pore-forming component leading to a nanoporous internal structure of the microparticles. Furthermore, TA/PVP particles are non-cytotoxic, are efficiently phagocytosed by DCs in vitro and strongly promote cross-presentation to CD8 T cells in vitro. Immunization experiments in mice have shown that encapsulation of vaccine protein antigens promotes, relative to soluble antigen, the antigen-specific humoral and cellular immune response in vivo.

Compared to vaccine nano- and microparticle formulations that contain in addition to antigen also molecular adjuvants (i.e., molecular adjuvants such as Toll like receptor agonists (e.g., CpG and MPLA)) that strongly activate antigen presenting cells, the observed immune responses are still modest. However, due to the versatility of our encapsulation procedure it will be straightforward to encapsulate such molecular adjuvants within the microparticles. Taken together, we believe that this type of delivery system has the potential to be further developed for (co)formulation of immune-stimulating cues, clinically relevant antigens against intracellular pathogens and for anti cancer immune therapy. Additionally, as a dry powder formulation is produced, this formulation avoids the cold chain, thereby offering potential for the formulation of pandemic vaccines or vaccines intended for the developing world that both suffer from logistic issues under refrigerated conditions.

4. Experimental Section

Materials: Poly(N-vinylpyrrolidone) (Kollidon12) was purchased from BASF. Tannic acid, N-vinyl pyrrolidone (NVP), azobisisobutyronitrile (AIBN), fluorescein-o-acrylate, dimethylacetamide (DMA), dichloromethane and Hoechst were purchased from Sigma-Aldrich. Mannitol was purchased from Cargill. AlexaFluor488 conjugated ovalbumin (OVA-AF488), DQ-OVA and AlexaFluor647 conjugated cholera toxin subunit B (CTB-AF647) were purchased from Life Technologies. The xanthate CTA [(S)-2-(ethyl propionate)-(O-ethyl xanthate)] was synthesized according to the literature procedure.[39]

Synthesis of Fluorescent PVP (PVP-FITC): NVP (2 g), xanthate CTA (26.7 mg) [(S)-2-(ethyl propionate)-(O-ethyl xanthate)] and AIBN (5.91 mg) and 6 mL anisole were added to a Schlenk flask at a molar ratio of monomer/CTA/AIBN of 150/1/0.3. After degassing by 3 freeze-pump-thaw cyles the Schenk flask was placed in an oil bath set at 60 °C for 2 h. Subsequently, the reaction was quenched by immersion in an ice bath and exposure to air. The reaction mixture was then precipitated in hexane, dissolved in dichloromethane and re-precipitated in hexane for in total 3 times and recovered as a white powder. GC analysis indicated a $M_{n,th}$ of 11.4 kDa (based on conversion) while size exclusion chromatography (SEC) in DMA indicated a $M_{n,SEC}$ = 7.0 kDa and a dispersity ($Đ$) of 1.27. The reaction scheme is shown in Scheme 3. For fluorescent labeling, 50 mg of PVP and 10 mg of fluorescent-o-acrylate were dissolved in 2 mL and 1 mL of DMF, respectively, in Schlenk flasks. Prior to modification, the two solutions and propyl amine were degassed via 4 freeze-pump-thaw cycles. Subsequently, 1 mL of degassed propyl amine was added to PVP solution under N_2 atmosphere and stirred for 2 h at room temperature to deprotect the thiol end-group of the PVP by aminolysis. Next, the excess of propylamine was removed by rotary evaporation. The reaction mixture was then again degassed and the fluorescein-o-acrylate solution was added by syringe under N_2 atmosphere and stirred overnight at room temperature. After dialysis against MilliQ water for 4 days and lyophilization, a fluffy orange colored powder was obtained. SEC was performed on a Agilent 1260-series HPLC system equipped with a 1260 online degasser, a 1260 ISO-pump, a 1260 automatic liquid sampler, a thermostated column compartment, a 1260 diode array detector (DAD) and a 1260 refractive index detector (RID). Analyses were performed on a PSS Gram30 column in series with a PSS Gram1000 column at 50 °C. DMA containing 50 mM of LiCl was used as eluent at a flow rate of 0.593 mL/min. The spectra were analysed using the Agilent Chemstation software with the GPC add on. Molar mass and dispersity ($Đ$) values were calculated against PMMA standards.

Quartz Crystal Microbalance: QCM measurements were performed on a Gamry eQCM equipped with an ALS flow cell. Gold coated quartz chips were first coated by 1 h immersion in an aqueous solution of mercaptosuccinic acid (2 mg/mL) followed by extensive rinsing with water. Secondly, the quartz chip was immersed into an aqueous PEI solution (2 mg/mL) for 1 h and again extensively washed with water and dried under a gentle nitrogen stream. Next, the chip was mounted into the flow cell, water was injected and the measurement was started and continued until a flat baseline was obtained. Then the measurement was restarted and after 100 s 200 µL of tannic acid (TA; 2 mg/mL in water) was injected. 100 s later, 500 µL of water was injected to remove the non-adsorbed TA. 100 s later PVP (2 mg/mL in water) was injected and after 100 s again 500 µL of water was injected. This procedure was repeated until a total of 10 TA/PVP bilayers were deposited.

Preparation of TA/PVP Microparticles via Spray Drying: Mannitol, PVP, OVA and TA were mixed in water in a 40:10:1:10 ratio and a total solid concentration of 0.5%. Three different adding sequences were evaluated. First sequence: 400 mg of mannitol, 10 mg of OVA and 50 mg of PVP were dissolved in 92 mL water. Subsequently 10 mL water containing 50 mg TA was added dropwise under stirring. Second sequence: 400 mg mannitol and 50 mg PVP were dissolved in 90 mL water, then 10 mL water containing 50 mg TA was added dropwise followed by the addition of 2 mL water containing 10 mg OVA. Both additions proceeded under stirring. Third sequence: 400 mg mannitol and 10 mg OVA were dissolved in 82 mL water. Next 10 mL water containing 50 mg of TA was added dropwise followed by the addition of 10 mL of water containing 50 mg of PVP. Both additions proceeded under stirring. Fluorescently labelled particles were prepared using either a mixture of OVA with Alexa488 conjugated ovalbumin or PVP with PVP-fluorescein, both in a 10:1 ratio. Spray drying was performed with a lab-scale Buchi B290 spray-dryer equipped with a two fluid nozzle (0.7 mm diameter). The setting of the inlet temperature was 120 °C and gas flow 0.55 bar. The mixtures were fed via a peristaltic feed pump at a feed flow of 2.4 mL/min. Dry powder was collected.

Encapsulation Efficiency: The quantification of encapsulation efficiency was determined by resuspending a known amount of microspheres (OVA-AF488, PVP-fluorescein microspheres and non-labelled microspheres to measure respectively OVA, PVP and TA encapsulation) in phosphate buffered saline (PBS) followed by centrifugation and measuring the amount of non-encapsulated OVA-AF488, PVP-fluorescein or TA in the supernatant. For OVA-AF488 and PVP-fluorescein this was done via fluorescence spectrometry using a Perkin-Elmer Envision multilabel plate reader. TA concentration was measured via UV-VIS spectrophotometry at 280 nm.

Microscopy: Scanning Electron Microscopy (SEM) was conducted on a Quanta 200 FEG FEI scanning electron microscope. Samples were sputtered with a palladium-gold layer prior to imaging. Transmission electron microscopy was performed on a JEOL 1010 instrument. Porosity of the particles was assessed using ImageJ (NIH) by binarizing the TEM images followed by calculating the ratio of black to white pixels within a circular region of interest which comprises the microparticle section. Confocal microscopy was conducted on a Leica SP5 microscope equipped with a 63X oil immersion objective. DC2.4 cells were plated a density of 50 000 per well in 8 well Ibidi chambers and incubated overnight with 5 µL of a 25 mg/mL microparticle suspension. CTB-647 and Hoechst staining was performed according to the manufactures' instructions.

Cell Lines and Animals: C57BL/6 mice were obtained from Janvier. OT-I transgenic mice (C57BL/6) were purchased from Harlan. Mice were housed under specific-pathogen-free conditions. All animal experiments were approved by the Local Ethical Committee of Ghent University. The immortalized mouse dendritic cell line DC2.4 was a kind gift from Prof. Dr. Ken Rock (Dana-Farber Cancer Institute, Boston, MA, USA). Bone-marrow-derived DCs were generated by flushing tibia and femurs of 2–4 months old C57BL/6 mice. After red blood cell lysis, cells were cultured in complete RPMI (Roswell Park Memorial Institute) medium containing 20 ng/mL GM-CSF (granulocyte macrophage colony-stimulating factor) for 6–8 days.

Cell Toxicity Assay: The cytotoxicity of the spray-dried particles was assessed according to De Koker et al.[40] DC2.4 cells were grown and seeded in 96-well plate at a density of 5×10^3 cells/well and incubated with different concentrations of the respective samples for 6 h. Afterwards, the medium was refreshed and cells were cultured for another 48 h. Medium was removed and MTT (3-(4,5-dimethylthiazol-2-yl)-2,5-diphenyltetrazolium bromide) was added. MTT is reduced by mitochondrial dehydrogenases of living cells into an insoluble purple formazan dye. After 3 hours of incubation at 37 °C, cells are solubilized by dimethylsulfoxide (DMSO) and the released, solubilized formazan is measured spectrophotometrically at 590 nm. The absorbance is a measure of the viability of the cells.

In Vitro Antigen-Presentation Assay: Cell suspensions of OVA-specific CD8 T cells were prepared from spleen and lymph nodes from OT-I mice. Single cell suspensions were prepared, and CD8 T cells were isolated from the suspensions using Dynal mouse CD8 negative isolation kit (Invitrogen) according to the manufacturer's instructions and subsequently labeled with CFSE (carboxyfluorescein diacetate succinimidyl ester). DCs obtained from bone marrow of C57BL/6 mice were pulsed with serial dilutions of the respective samples for 24 h, washed, counted and subsequently co-cultured with OT-I T cells at different DC:T cell ratios for 48 h. After 48 h, the division of the OT-I T cells was measured by flow cytometry using a BD LSR II.

Readout of In Vivo Antibody Response (ELISA): Mice were vaccinated twice with a 3 week interval with 100 µL containing 50 µg of either soluble or encapsulated OVA. For the detection of anti-OVA antibodies. Blood samples were collected from the ventral tail vein. Maxisorp (Nunc) plates were coated with OVA (10 mg/mL) and incubated with serial dilutions of serum. Antibody titers were subsequently detected with goat anti-mouse IgG1-HRP (Southern Biotech; HRP = horse-raddish peroxidase) and goat anti-mouse IgG2c-HRP (Southern Biolabs), respectively. Data show antibody titers of individual mice.

Readout of In Vivo Cellular Response (ELISPOT): Splenocytes were harvested three weeks after the booster immunization. Suspensions of 2×10^5 splenocytes were cultured onto IFN-γ ELISPOT plates (Diaclone) in triplicate and restimulated with 5 mg/mL of either the OVA MHCI epitope peptide SIINFEKL or the OVA MHCII epitope peptide ISQAVHAAHAEINEAGR (both Anaspec). ELISPOTs were developed after a 24 h incubation period.

Supporting Information

Supporting Information is available from the Wiley Online Library or from the author.

Acknowledgements

B.D.G. and M.D. acknowledge Ghent University (BOF-GOA) for funding. B.D.G. and R.H. acknowledge the FWO-Flanders for research grants. S.M. gratefully acknowledges FWO for the Pegasus Marie Curie Fellowship. Z.Z. and Q.Z. acknowledge the CSC and Ghent University (BOF-CSC-co-funding) for a PhD scholarship. The authors gratefully acknowledge Dr. Ken Rock for providing the DC2.4 cell line.

Received: March 7, 2014
Published online: April 30, 2014

[1] A. Luchini, D. H. Geho, B. Bishop, D. Tran, C. Xia, R. L. Dufour, C. D. Jones, V. Espina, A. Patanarut, W. Zhou, M. M. Ross, A. Tessitore, E. F. Petricoin, L. A. Liotta, *Nano Lett.* **2008**, *8*, 350.
[2] N. Murthy, M. C. Xu, S. Schuck, J. Kunisawa, N. Shastri, J. M. J. Frechet, *Proc. Natl. Acad. Sci. U.S.A.* **2003**, *100*, 4995.
[3] J. W. Yoo, D. J. Irvine, D. E. Discher, S. Mitragotri, *Nat. Rev. Drug Discovery* **2011**, *10*, 521.
[4] J. A. Hubbell, S. N. Thomas, M. A. Swartz, *Nature* **2009**, *462*, 449.
[5] S. De Koker, R. Hoogenboom, B. G. De Geest, *Chem. Soc. Rev.* **2012**, *41*, 2867.
[6] J. J. Moon, B. Huang, D. J. Irvine, *Adv. Mater.* **2012***24*, 3724.
[7] R. Rappuoli, *Nat. Med.* **2004**, *10*, 1177.
[8] B. G. De Geest, M. A. Willart, H. Hammad, B. N. Lambrecht, C. Pollard, P. Bogaert, M. De Filette, X. Saelens, C. Vervaet, J. P. Remon, J. Grooten, S. De Koker, *ACS Nano* **2012**, *6*, 2136.
[9] B. G. De Geest, M. A. Willart, B. N. Lambrecht, C. Pollard, C. Vervaet, J. P. Remon, J. Grooten, S. De Koker, *Angew. Chem. Int. Ed.* **2012**, *51*, 3862.
[10] S. T. Reddy, A. J. van der Vlies, E. Simeoni, V. Angeli, G. J. Randolph, C. P. O'Neill, L. K. Lee, M. A. Swartz, J. A. Hubbell, *Nat. Biotechnol.* **2007**, *25*, 1159.
[11] Y. J. Kwon, E. James, N. Shastri, J. M. J. Frechet, *Proc. Natl. Acad. Sci. U.S.A.* **2005**, *102*, 18264.
[12] J. J. Moon, H. Suh, A. V. Li, C. F. Ockenhouse, A. Yadava, D. J. Irvine, *Proc. Natl. Acad. Sci. U.S.A.* **2012**, *109*, 1080.
[13] J. J. Moon, H. Suh, A. Bershteyn, M. T. Stephan, H. P. Liu, B. Huang, M. Sohail, S. Luo, S. H. Um, H. Khant, J. T. Goodwin, J. Ramos, W. Chiu, D. J. Irvine, *Nat. Mater.* **2011**, *10*, 243.
[14] S. De Koker, B. G. De Geest, S. K. Singh, R. De Rycke, T. Naessens, Y. Van Kooyk, J. Demeester, S. C. De Smedt, J. Grooten, *Angew. Chem. Int. Ed.* **2009**, *48*, 8485.
[15] S. P. Kasturi, I. Skountzou, R. A. Albrecht, D. Koutsonanos, T. Hua, H. I. Nakaya, R. Ravindran, S. Stewart, M. Alam, M. Kwissa, F. Villinger, N. Murthy, J. Steel, J. Jacob, R. J. Hogan, A. Garcia-Sastre, R. Compans, B. Pulendran, *Nature* **2011**, *470*, 543.
[16] M. Dierendonck, S. De Koker, C. Cuvelier, J. Grooten, C. Vervaet, J. P. Remon, B. G. De Geest, *Angew. Chem. Int. Ed.* **2010**, *49*, 8620.
[17] M. Dierendonck, S. De Koker, R. De Rycke, P. Bogaert, J. Grooten, C. Vervaet, J. P. Remon, B. G. De Geest, *ACS Nano* **2011**, *5*, 6886.
[18] B. Devriendt, K. Baert, M. Dierendonck, H. Favoreel, S. De Koker, J. P. Remon, B. G. De Geest, E. Cox, *Eur. J. Pharm. Biopharm.* **2013**, *84*, 421.
[19] F. Caruso, R. A. Caruso, H. Mohwald, *Science* **1998**, *282*, 1111.
[20] G. Decher, *Science* **1997**, *277*, 1232.
[21] E. Donath, G. B. Sukhorukov, F. Caruso, S. A. Davis, H. Mohwald, *Angew. Chem. Int. Ed.* **1998**, *37*, 2202.
[22] S. Setia, H. Mainzer, M. L. Washington, G. Coil, R. Synder, B. G. Weniger, *Vaccine* **2002**, *20*, 1148.
[23] H. P. S. Makkar, M. Blummel, K. Becker, *Br. J. Nutr.* **1995**, *73*, 897.
[24] I. Erel-Unal, S. A. Sukhishvili, *Macromolecules* **2008**, *41*, 3962.

[25] V. Kozlovskaya, O. Zavgorodnya, Y. Chen, K. Ellis, H. M. Tse, W. X. Cui, J. A. Thompson, E. Kharlampieva, *Adv. Funct. Mater.* **2012**, *22*, 3389.
[26] V. Kozlovskaya, E. Kharlampieva, I. Drachuk, D. Cheng, V. V. Tsukruk, *Soft Matter* **2010**, *6*, 3596.
[27] T. S. Sileika, D. G. Barrett, R. Zhang, K. H. Lau, P. B. Messersmith, *Angew. Chem. Int. Ed.* in press
[28] Z. C. Zhu, N. Gao, H. J. Wang, S. A. Sukhishvili, *J. Controlled Release* **2013**, *171*, 73.
[29] A. Shukla, J. C. Fang, S. Puranam, F. R. Jensen, P. T. Hammond, *Adv. Mater.* **2012**, *24*, 492.
[30] B. S. Kim, H. Lee, Y. H. Min, Z. Poon, P. T. Hammond, *Chem. Commun.* **2009**, 4194.
[31] A. B. F. Antunes, M. Dierendonck, G. Vancoillie, J. P. Remon, R. Hoogenboom, B. G. De Geest, *Chem. Commun.* **2013**, *49*, 9663.
[32] H. Ejima, J. J. Richardson, K. Liang, J. P. Best, M. P. van Koeverden, G. K. Such, J. W. Cui, F. Caruso, *Science* **2013**, *341*, 154.
[33] J. F. Quinn, A. P. R. Johnston, G. K. Such, A. N. Zelikin, F. Caruso, *Chem. Soc. Rev.* **2007**, *36*, 707.
[34] G. K. Such, A. P. R. Johnston, F. Caruso, *Chem. Soc. Rev.* **2011**, *40*, 19.
[35] Y. Gonnissen, J. P. Remon, C. Vervaet, *Eur. J. Pharm. Biopharm.* **2007**, *67*, 220.
[36] K. J. Siebert, N. V. Troukhanova, P. Y. Lynn, *J. Agric. Food Chem.* **1996**, *44*, 80.
[37] S. Perrier, P. Takolpuckdee, *J. Polym. Sci. A Polym.* **2005**, *43*, 5347.
[38] H. Willcock, R. K. O'Reilly, *Polym. Chem.1*, 149.
[39] G. Pound, Z. Eksteen, R. Pfukwa, J. M. McKenzie, R. F. M. Lange, B. Klumperman, *J. Polym. Sci. A Polym.* **2008**, *46*, 6575.
[40] S. De Koker, B. G. De Geest, C. Cuvelier, L. Ferdinande, W. Deckers, W. E. Hennink, S. De Smedt, N. Mertens, *Adv. Funct. Mater.* **2007**, *17*, 3754.